High-Isolation X-Band Marine Radar Antenna Design

Fang-Yao Kuo, *Student Member, IEEE*, and Ruey-Bing Hwang, *Senior Member, IEEE*

***Abstract*—This paper presents a high-isolation printed antenna array for marine radar applications. The antenna array is composed of 32 identical square microstrip patches operated at a center frequency of 9.35 GHz and includes a 100-MHz bandwidth (subject to a 1.5:1 voltage standing wave ratio [VSWR]). The patch antennas are arranged in four arms, each of which contains eight elements and is series-fed using Chebyshev tapering (25 dB side-lobe level). To apply the antenna in marine radar applications, an antenna with horizontal polarization was employed because, in comparison with vertical polarization, it can relatively reduce the sea clutter reflectivity. Therefore, a slit was carved on each patch element to change the current path, thereby enabling horizontal polarization. The antenna gain, 3-dB beamwidth, side-lobe level, and front-to-back ratio were 22 dBi, 5.3°, 26.4 dB, and 38.5 dB, respectively. Additionally, metallic baffles were introduced for increasing the isolation between the transmitting and receiving antennas to 60 dB.**

***Index Terms*—High isolation, horizontal polarization, marine radar, printed antenna array.**

I. Introduction

MARINE radars are essential sensors used for detecting hazards (such as coastlines, icebergs, or other ships), and assisting the navigator in making timely decisions. Currently, several frequency bands are assigned to marine radar applications, including the S, X, and Ku bands; in this research, the operating bandwidth ranges from 9.3 to 9.4 GHz. Compared with the systems using S band, the X-band systems have the advantages of compactness, flexibility, and maneuverability, which benefit yachts and fishing boats.

Marine radar typically uses a high-gain antenna equipped with a rotator that scans the horizon by transmitting radio signals in known directions and receiving the returned echoes for detecting objects of interest [1]. Several factors that affect radar performance are caused by the antennas used; these factors are side-lobe level, front-to-back ratio, polarization, and main-beam width. For example, the signals transmitted from an antenna can illuminate scatterers through the side lobes or back lobe, and the reflection is picked up in the same manner in receiving mode. The undesired signals falsely display a target in the main-beam direction, thereby causing the error to be detected. Moreover, using antenna with horizontal polarization can relatively reduce the sea clutter reflectivity in comparison with using an antenna with vertical polarization [2]. Additionally, to resolve two targets in close proximity, applying a narrow beamwidth along the horizontal plane is necessary.

Microstrip patch array antennas are extensively applied in radar systems [3]–[7] and wireless communications systems [8]–[11], which are high gain, low cost, lightweight, and low profile, and can accurately control radiation patterns. Two types of array feeding structures are commonly used, namely parallel-fed and series-fed structures. Regarding the parallel-fed scheme, numerous power dividers containing many discontinuities and long transmission lines are required, the presence of which causes spurious radiation and substantial dielectric loss to occur [12]. Conversely, the series-fed structure uses short transmission lines and enhances antenna efficiency [13]. In the series-fed structure, resonant and traveling-wave feeds are commonly used. The bandwidth of a traveling-wave feed is wider than that of a resonant feed. However, the main-beam angle changes in accordance with the change in operation frequency, which is caused by the change in the progressive phase angle between two adjacent elements along the series-fed lines. This can cause inaccurate angle detection to occur, particularly in a frequency-modulated continuous-wave (FMCW) system. By contrast, the parallel-fed structure at the center of the array ensures that the combined beam of each half array remains pointed in the broadside direction [14], [15].

In this paper, a high-isolation printed array antenna used for marine radar applications is presented. An array consisting of 32 identical square microstrip patches operated at a center frequency of 9.35 GHz with a 100-MHz bandwidth (1.5:1 voltage standing wave ratio [VSWR]) was developed. The patch antennas were arranged along the four arms of a 1-D array containing eight elements, and center fed using a series of microstrip lines exhibiting Chebyshev taper distribution. Traveling-wave taper distribution was achieved using quarter-wavelength transformers along the line to reduce the side-lobe level to 25 dB below that of the main beam. A slit was carved on each patch element to change the current path, thereby enabling horizontal polarization. Moreover, individually loading the transmitting and receiving antennas with metallic baffles can increase the isolation between them to over 60 dB.

II. Array Configuration and Design Method

Fig. 1 shows the configuration of the developed array that was implemented on a 31-mil substrate with a dielectric constant of $\varepsilon_r = 2.2$ and a loss tangent of $\tan\delta = 0.0009$. This array consisted of a feeding network and 32 identical square microstrip patches operated at a center frequency of 9.35 GHz. As

Manuscript received September 13, 2013; revised January 16, 2014; accepted January 19, 2014. Date of publication February 20, 2014; date of current version May 01, 2014. This work was supported in part by the National Science Council under the contract number: NSC 101-2221-E-009-097-MY2.

The authors are with the Department of Electrical Engineering, National Chiao-Tung University, Hsinchu 300, Taiwan (e-mail: raybeam@mail.nctu.edu.tw).

Color versions of one or more of the figures in this paper are available online at http://ieeexplore.ieee.org.

Digital Object Identifier 10.1109/TAP.2014.2307296

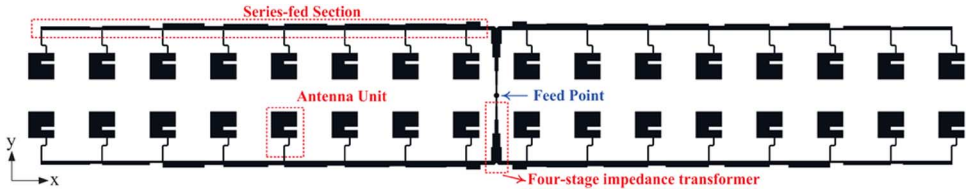

Fig. 1. Top view of the proposed antenna array, which was placed on a grounded substrate with a thickness of 31 mil and a dielectric constant $\varepsilon_r = 2.2$.

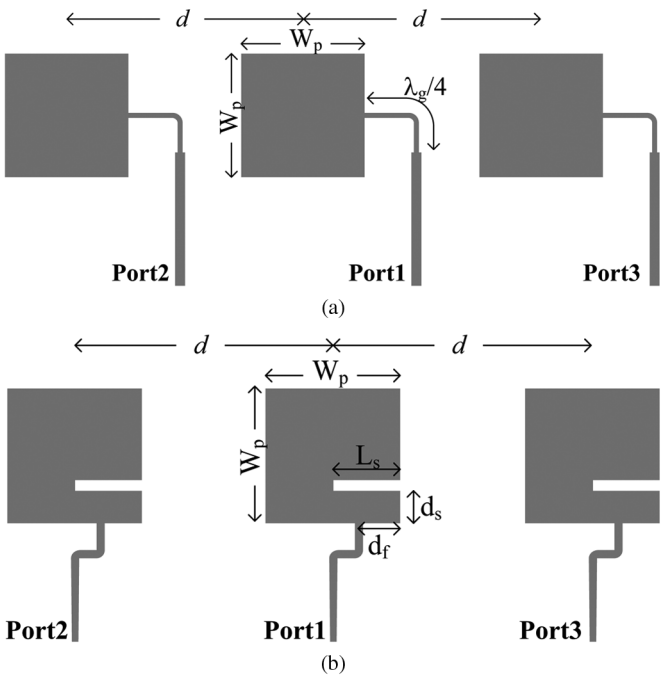

Fig. 2. Configurations of (a) a conventional antenna and (b) the proposed element antenna with horizontal polarization. The design parameters were $W_p = 9.9$ mm, $L_s = 5$ mm, $d_f = 2.455$ mm, and $d_s = 3$ mm.

shown in Fig. 1, the feeding network consisted of two T-junctions connected to each other and fed using a vertical probe. Each arm of the T-junction was connected to the series-fed patch array. For obtaining a favorable impedance match, a four-stage quarter-wavelength transformer was employed in the T-junction design. Owing to the head-to-head arrangement of the antenna arrays, the top and bottom array were subjected to out-of-phase currents. The electric-field component along the y-axis was cancelled out in the far field, thereby enabling the suppression of the cross-polarization level. In this study, a time-domain finite-integration-based electromagnetic simulation tool, CST Microwave Studio [16], was used for computing the radiating characteristics of the array antenna.

A. Antenna Element Design

Because the polarization of a microstrip patch antenna is inherently related to feeding position, the traditionally used method for obtaining horizontal polarization is feeding from the lateral edge of the patch, as shown in Fig. 2(a). However, the feed line in between the two patches causes strong coupling to occur, which subsequently reduces isolation and degrades the performance of the original patch. To maintain the feeding position at the bottom edge of the patch and enable horizontal polarization, a slit was carved on the patch element to enable

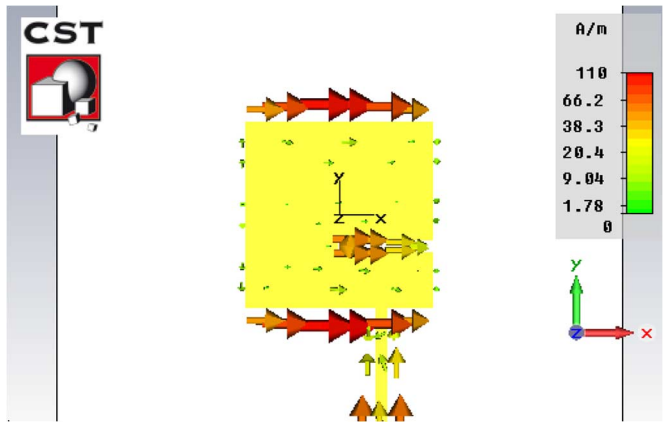

Fig. 3. Surface current density of the proposed patch element at 9.35 GHz.

the current to flow along the horizontal direction. An off-center microstrip line with 100 Ω characteristic impedance was adopted for impedance matching, as shown in Fig. 2(b).

Fig. 3 shows the surface current density of the proposed patch element at 9.35 GHz, which can verify the realization of horizontal polarization. The current was fed from the microstrip line on the lower right side of the patch. Because the current path along the vertical direction was interrupted by the slit, the current was compelled to flow along the horizontal direction. The current vectors on the edge and around the slit were headed along the horizon, thereby generating horizontal polarization. To investigate the effect of the slit length and placement on antenna performance further, parameter studies were conducted, as shown in Fig. 4. The cross-polarization level indicated how many decibels the power level of vertical polarization was below the power level of horizontal polarization in the main beam direction ($\theta = 0$, $\phi = 0$). In Fig. 4, the cross-polarization level increases as the length of the slit (L_s) and the distance of the slit from the patch's bottom edge (d_s) increase. Because the variation of the reflection coefficient is not as regular as that of the cross-polarization level, a tradeoff must be made between the reflection coefficient and cross-polarization level. Since the transmitted power is high for marine radar, the low reflection coefficient is needed for not damaging the transmitter.

Each patch antenna located in the arrays in Fig. 2 was designed to have a center frequency of 9.35 GHz; the reflection coefficients (S_{11}) are shown in Fig. 5. Using the proposed antenna exhibiting off-center feed and a horizontal slit did not affect the reflection coefficient considerably. In addition to the single element characteristic, the array performance, including cross-polarization and isolation, was compared between these two types of antenna. Fig. 6 shows the effect of the spacing between elements d on isolation and the cross-polarization level. The performance of the conventional patch was determined to

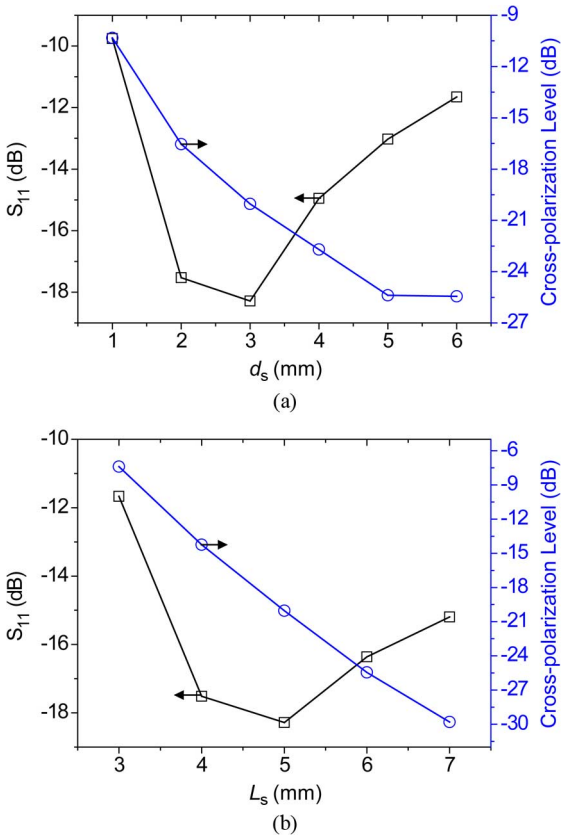

Fig. 4. Parametric sweep of the physical parameters (a) d_s and (b) L_s for investigating the effect of these parameters on the reflection coefficient and cross-polarization level of the antenna at 9.35 GHz.

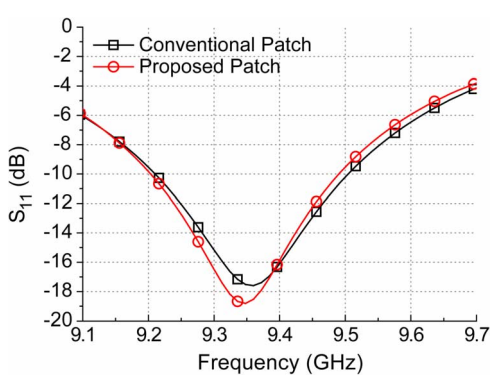

Fig. 5. Reflection coefficients (S_{11}) of the proposed and conventional antenna elements.

be more sensitive to spacing than that of the proposed patch element. The comparison of antenna gain and S_{11} is not shown because they exhibited similar trends.

B. Feeding Network

Fig. 7 shows the structure of the series-fed section. The spacing between the feed points of the patch elements was fixed to one guided wavelength for an equal phase delay between the elements. Lines with lengths $\lambda_g/4$ and $3\lambda_g/4$ were introduced between two consecutive outputs to obtain taper distribution at the output port (from Port 2 to N) and obtain minimal reflection at the input port (Port 1). The series-fed section can be regarded as a cascade of several T-junctions. The detailed electrical

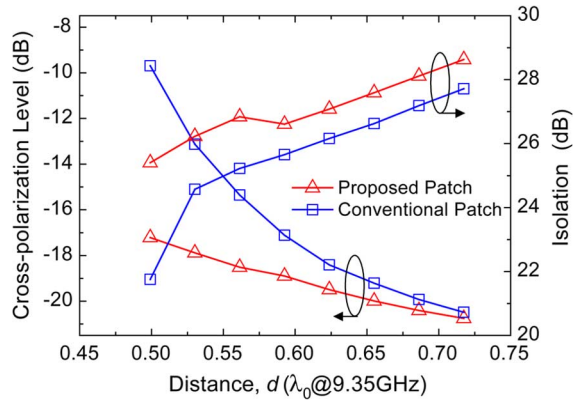

Fig. 6. Isolation and cross-polarization level as a function of the spacing between elements d for the proposed and conventional antenna arrays.

dimensions of the ith $(i = 2, 3, \ldots, 8)$ T-junction model are depicted in Fig. 8(a). The power ratio between Port 2 and Port 3 depends on the characteristic impedance of each connected microstrip line. To simplify the analysis of the feeding network further, the equivalent transmission-line network and the corresponding scattering matrices were constructed using the building block approach, as shown in Fig. 8(b) and (c), respectively, thereby reducing computing time considerably.

In Fig. 8(c), $\mathbb{S}^{Ta}$, $\mathbb{S}^{Tb}$, and $\mathbb{S}^{Tc}$ are the 2-by-2 scattering matrices of the ideally lossless transmission lines Ta, Tb, and Tc, respectively. These scattering matrices have been reported in the relevant literature and are widely recognized [17]. The 3-by-3 scattering matrix of an ideal T-junction Tj, shown in Fig. 8(c), can be expressed as

$$S_{ii} = \frac{Z_{in}^{(i)} - Z^{(i)}}{Z_{in}^{(i)} + Z^{(i)}}, \text{ for } i = 1, 2, 3 \tag{1}$$

$$S_{ij} = \frac{2Z_{in}^{(j)}\sqrt{\frac{Z^{(j)}}{Z^{(i)}}}}{Z_{in}^{(i)} + Z^{(i)}}, \text{ for } i, j = 1, 2, 3 \;\&\; i \neq j \tag{2}$$

where Z_{in} is the input impedance at the ith port with reference impedance $Z^{(i)}$, which is defined as

$$Z_{in}^{(i)} = Z^{(p)} \parallel Z^{(q)}, \text{ for } i, p, q = 1, 2, 3 \;\&\; i \neq p \neq q. \tag{3}$$

Because the detailed mathematical procedures used for deriving the scattering matrix of the T-junction network were described in [18], only the result is provided to maintain the conciseness of this paper. The three-port scattering matrix is given by

$$\mathbb{S} = \mathbb{S}_{pp} + \mathbb{S}_{pc}(\mathbb{M} - \mathbb{S}_{cc})^{-1}\mathbb{S}_{cp}, \tag{4}$$

where matrixes $\mathbb{S}_{pp}$, $\mathbb{S}_{pc}$, $\mathbb{S}_{cp}$, $\mathbb{S}_{cc}$, and $\mathbb{M}$ are given below by

$$\mathbb{S}_{pp} = \begin{bmatrix} S_{11}^{Ta} & 0 & 0 \\ 0 & S_{22}^{Tb} & 0 \\ 0 & 0 & S_{22}^{Tc} \end{bmatrix} \tag{5}$$

$$\mathbb{S}_{pc} = \begin{bmatrix} S_{12}^{Ta} & 0 & 0 & 0 & 0 & 0 \\ 0 & S_{21}^{Tb} & 0 & 0 & 0 & 0 \\ 0 & 0 & S_{21}^{Tc} & 0 & 0 & 0 \end{bmatrix} \tag{6}$$

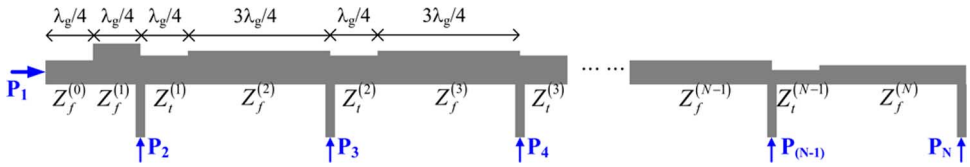

Fig. 7. Configuration and definition of parameters for the series-fed section shown in Fig. 1.

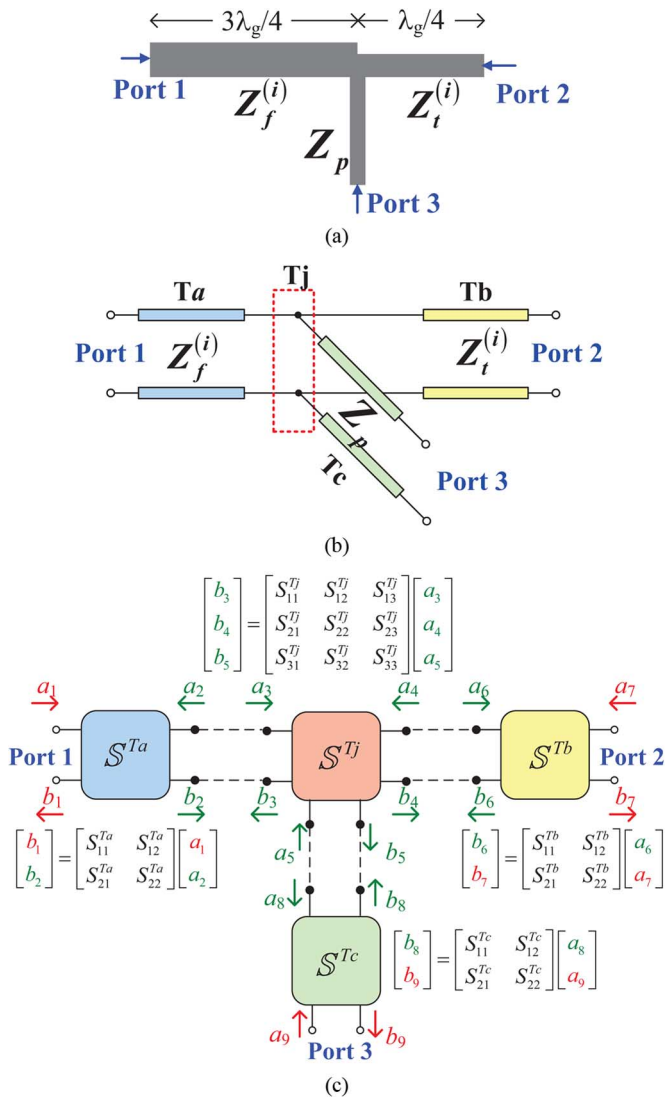

Fig. 8. (a) Electrical dimensions, (b) ideal transmission line model, and (c) building blocks for the ith ($i = 2, 3, \ldots, 8$) T-junction model.

$$\mathbb{S}_{cc} = \begin{bmatrix} S_{22}^{Ta} & 0 & 0 & 0 & 0 & 0 \\ 0 & S_{11}^{Tb} & 0 & 0 & 0 & 0 \\ 0 & 0 & S_{11}^{Tc} & 0 & 0 & 0 \\ 0 & 0 & 0 & S_{33}^{Tj} & S_{32}^{Tj} & S_{31}^{Tj} \\ 0 & 0 & 0 & S_{23}^{Tj} & S_{22}^{Tj} & S_{21}^{Tj} \\ 0 & 0 & 0 & S_{13}^{Tj} & S_{12}^{Tj} & S_{11}^{Tj} \end{bmatrix} \tag{7}$$

$$\mathbb{S}_{cp} = \begin{bmatrix} S_{21}^{Ta} & 0 & 0 \\ 0 & S_{12}^{Tb} & 0 \\ 0 & 0 & S_{12}^{Tc} \\ 0 & 0 & 0 \\ 0 & 0 & 0 \\ 0 & 0 & 0 \end{bmatrix} \tag{8}$$

TABLE I
OPTIMIZED CHARACTERISTIC IMPEDANCES OF EACH LINE IN A SERIES-FED SECTION AND THE CORRESPONDING WIDTHS OF THE MICROSTRIP LINE

$Z_f^{(0)}$	65.9 (1.53)	$Z_t^{(1)}$	50.7 (2.35)
$Z_f^{(1)}$	40.2 (3.3)	$Z_t^{(2)}$	54.5 (2.10)
$Z_f^{(2)}$	48.0 (2.55)	$Z_t^{(3)}$	57.8 (1.91)
$Z_f^{(3)}$	49.0 (2.47)	$Z_t^{(4)}$	61.8 (1.71)
$Z_f^{(4)}$	49.2 (2.46)	$Z_t^{(5)}$	64.5 (1.59)
$Z_f^{(5)}$	50 (2.41)	$Z_t^{(6)}$	92 (0.80)
$Z_f^{(6)}$	47 (2.61)	$Z_t^{(7)}$	77.4 (1.14)
$Z_f^{(7)}$	62.6 (1.67)	unit:Ω (mm)	
$Z_f^{(8)}$	67.4 (1.47)		

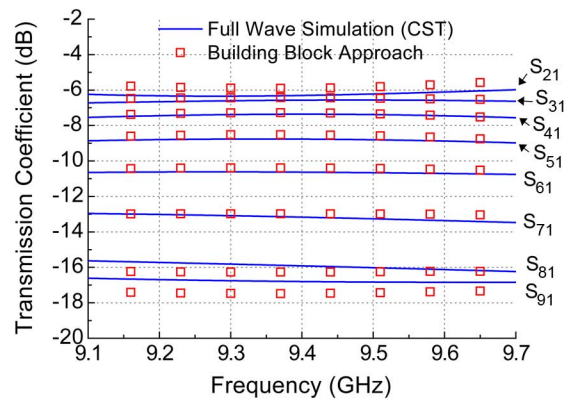

Fig. 9. Simulated amplitude characteristic of the series-fed section shown in Fig. 7 determined using a full-wave simulation tool and the building block approach.

$$\mathbb{M} = \begin{bmatrix} 0 & 0 & 0 & 0 & 0 & 1 \\ 0 & 0 & 0 & 0 & 1 & 0 \\ 0 & 0 & 0 & 1 & 0 & 0 \\ 0 & 0 & 1 & 0 & 0 & 0 \\ 0 & 1 & 0 & 0 & 0 & 0 \\ 1 & 0 & 0 & 0 & 0 & 0 \end{bmatrix}. \tag{9}$$

Similarly, the scattering matrix of the series-fed section shown in Fig. 7 can be determined by progressively cascading the S-matrices of each T-junction network. The two constraints, the Chebyshev tapering coefficients on the output ports and low return loss, were set to perform the optimization process by using a genetic algorithm; the optimized characteristic impedances and the corresponding widths of the microstrip line are summarized in Table I. Fig. 9 shows the simulated results derived using a full-wave simulation tool and the building block approach. The results were clearly similar and tapered amplitude distribution was achieved.

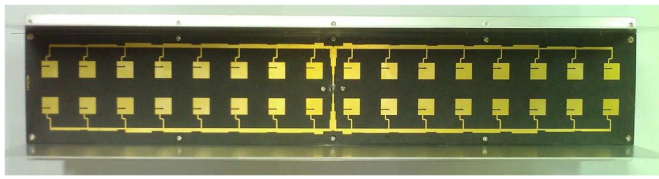

Fig. 10. Photograph of the proposed antenna.

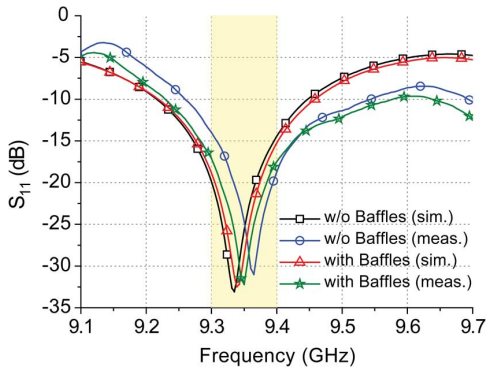

Fig. 11. Measured and simulated reflection coefficient results for the proposed array with and without baffles.

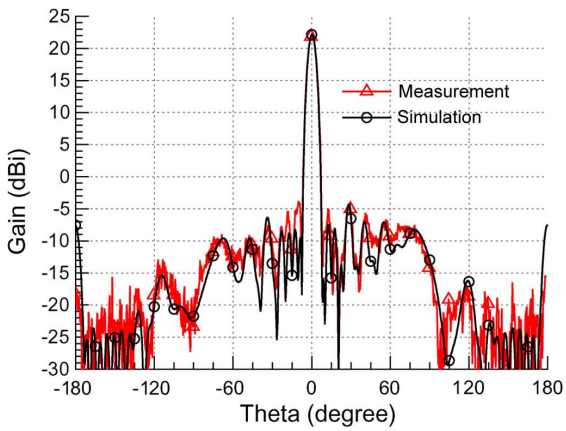

(a)

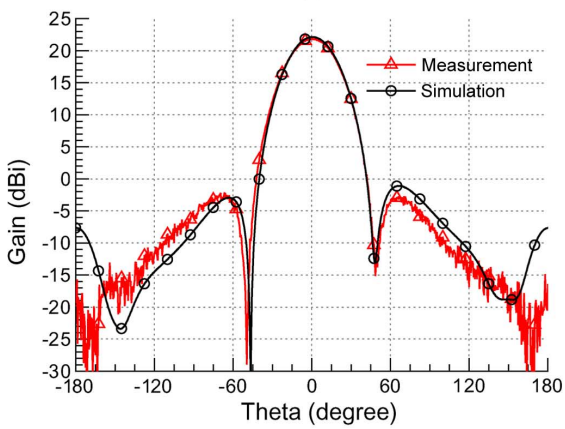

(b)

Fig. 12. Measured and simulated radiation patterns at 9.35 GHz on (a) a horizontal plane (yz-plane) and (b) a vertical plane (yz-plane).

III. Measurement Results and Discussion

A prototype of the developed antenna array was fabricated using PCB technology and the radiation characteristics of the antennas were measured. A photograph of the proposed antenna is shown in Fig. 10; the dimensions of the antenna were

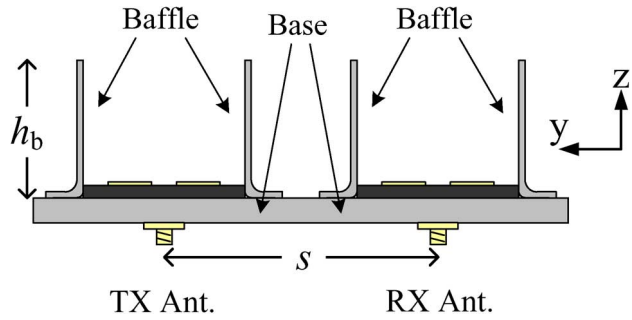

Fig. 13. Arrangement of the transmission and receiving antennas with a spacing s.

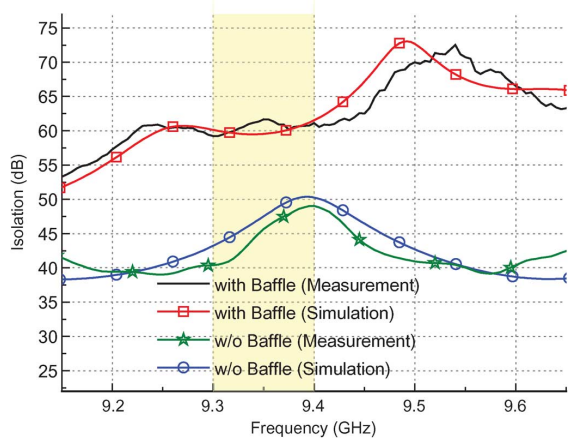

Fig. 14. Simulated and measured isolation for the array with baffles with $s = 85$ mm. The results for the array without baffles are also shown for comparison.

376 mm × 68.8 mm. The measured and simulated reflection coefficients are shown in Fig. 11 (curves labeled as "w/o Baffles"). The impedance bandwidth for −14 dB S_{11} (1.5:1 VSWR) was 9.26–9.4 GHz for the measured result and 9.3–9.44 GHz for the simulated result. These results agree with the trend (except for a slight frequency shift that occurred) and, thus, the impedance bandwidths are able to cover the desired frequency band from 9.3 to 9.4 GHz. Fig. 12 shows the measured and simulated radiation patterns produced by the proposed antenna at 9.35 GHz. On the horizontal plane (xz-plane) in Fig. 12(a), the measured antenna gain, half-power beamwidth, side-lobe level, and front-to-back ratio were 22 dBi, 5.3°, 26.4 dB, and 38.5 dB, respectively. The half-power beamwidth and side-lobe level on the vertical plane (yz-plane) were 34.5° and 23.7 dB, respectively.

Fig. 13 shows the arrangement of the transmitting and receiving antennas with a spacing (s) between them. The high-gain antenna focuses power on a narrow beamwidth, thereby reducing the amount of field coupling that occurred between antennas in close proximity. To improve the isolation further, metallic baffles were equipped and connected to the ground plane on both sides of the array. The length and height (h_b) of each metallic baffle were 376 mm and 50 mm, respectively. Fig. 14 shows the simulated and measured isolation when the baffles were used; for comparison, Fig. 14 also includes the results obtained when baffles were not used. The baffles clearly produced more than 10 dB of additional isolation (the difference [in dB] between the blue and red curves). However, the effect of the linear taper baffles on the reflection coefficient (S_{11})

TABLE II
MEASURED RESULTS FOR THE PROPOSED ANTENNA ARRAY

		w/o Baffles			with Baffles		
		9.3 GHz	9.35 GHz	9.4 GHz	9.3 GHz	9.35 GHz	9.4 GHz
Gain (dBi)		21.1	22	22.1	21.9	22.7	22.7
SLL (dB)		27.3	26.4	26.6	21.5	24.1	26.3
F/B (dB)		41.1	38.5	37.5	42	43.6	43.5
HPBW	horizontal-plane (xz-plane)	5.8°	5.3°	5.2°	5.6°	5.3°	5.2°
	vertical-plane (xz-plane)	35°	34.5°	33.5°	29°	28.9°	29.5°
Cross-polarization Level (dB)		−36.3	−35.8	−35.9	−35.4	−36.9	−38.8

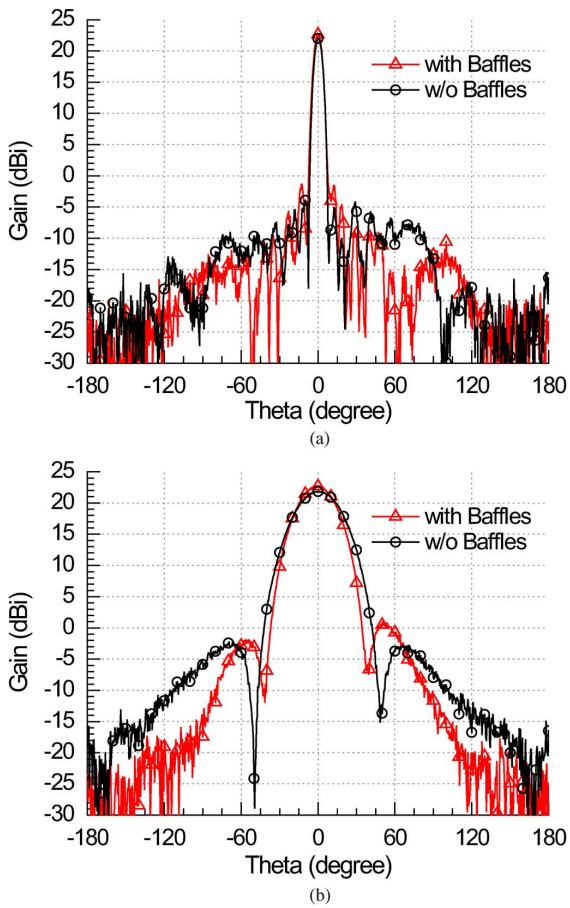

Fig. 15. Measured radiation patterns at 9.35 GHz on (a) a horizontal plane (xz-plane) and (b) a vertical plane (yz-plane).

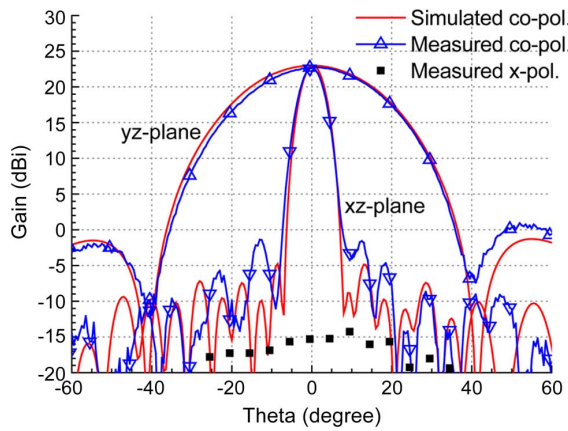

Fig. 16. Simulated and measured radiation pattern of the proposed antenna with baffles.

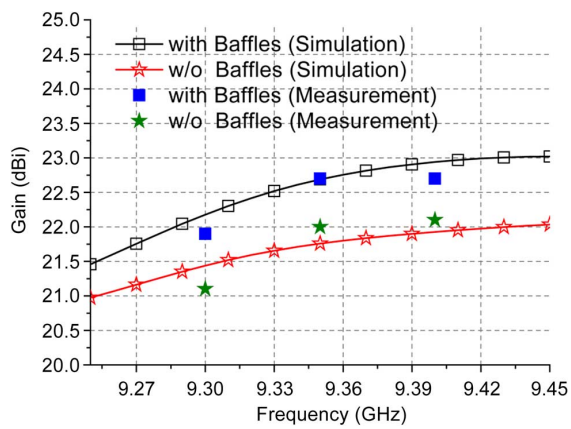

Fig. 17. Simulated and measured gains of the proposed array for various frequencies when the baffles were used and not used, respectively.

was negligible [19]. As shown in Fig. 11, the reflection coefficients of the proposed array with and without baffles were extremely similar. Regarding the radiation pattern, the supplementary baffle slightly increased the gain and enhanced the front-to-back ratio, as shown in Fig. 15. On the vertical plane (yz-plane) in Fig. 15(b), the half-power beamwidth became narrower. The side-lobe level on the horizontal plane (xz-plane) in Fig. 15(a) increased by 2 dB, compared with that of the proposed antenna without baffles. This can be ascribed to the deformation of the printed circuit board caused by the stress of the screws, which resulted in the degradation of side-lobe performance. Fig. 16 shows the simulated and measured radiation patterns of the proposed antenna with baffles. The maximal strength of cross-polarization was −36.9 dB below that of co-polarization. This low cross-polarization level was contributed by the symmetric 1-D array with respect to the x-axis. Fig. 17 shows the simulated and measured gain of the proposed array when the baffles were used and not used, respectively. The trends of the measurement are close to those of the simulation. The measurement results for the radiation characteristics are summarized in Table II.

IV. Conclusion

A high-isolation printed antenna array for marine radar applications was designed and fabricated, and the radiation characteristics were measured. The array was composed of 32 identical square microstrip patches arranged along the four arms of a 1-D array containing eight elements. By using the series-fed structure with Chebyshev tapering, the side-lobe level was suppressed. Moreover, the symmetric design with respect to the x-axis substantially suppressed the cross-polarization level. Compared with the conventional patch element design, the novel design proposed in this study with a slit and off-center feed mitigated the electromagnetic coupling that occurred through the feed-line to patch coupling. Furthermore, applying the metallic baffles to the exterior of the antennas substantially enhanced the isolation between the transmitting and receiving antennas. The measured and simulated results agree well. Additionally, the electrical performance of the developed antenna is able to meet the specifications of the antennas applied in marine radar systems.

Acknowledgment

The authors would like to thank the support of CST in providing software for numerical simulation.

References

[1] M. I. Skolnik, *Radar Handbook*. New York, NY, USA: McGraw-Hill, 1970.
[2] J. N. Briggs, *Target Detection by Marine Radar*. London, U.K.: The Institution of Electrical Engineers, 2004.
[3] Y.-B. Jung, I. Yeom, and C. W. Jung, "Centre-fed series array antenna for k-/ka-band electromagnetic sensors," *IET Microw., Antennas, Propag.*, vol. 6, no. 5, pp. 588–593, Apr. 2012.
[4] M. Hajian, J. Zijderveld, A. A. Lestari, and L. P. Ligthart, "Analysis, design and measurement of a series-fed microstrip array antenna for X-band INDRA: The Indonesian maritime radar," in *Proc. 3rd Eur. Conf. Antennas Propag.*, Berlin, Germany, Apr. 2009, pp. 1154–1157.
[5] T. Huque, K. Hossain, S. Islam, and A. Chowdhury, "Design and performance analysis of microstrip array antennas with optimum parameters for X-band applications," *Int. J. Adv. Comput. Sci. Applicat.*, vol. 2, no. 4, pp. 81–87, 2011.
[6] J. Hautcoeur, E. M. Cruz, J. Bartholomew, J. Sarrazin, Y. Mahe, and S. Toutain, "Low-cost printed antenna array built with hybrid feed for urban microwave links," *IET Microw., Antennas, Propag.*, vol. 4, no. 9, pp. 1320–1326, Sep. 2010.
[7] H. Iizuka, K. Sakakibara, T. Watanabe, K. Sato, and K. Nishikawa, "Millimeter-wave microstrip array antenna with high efficiency for automotive radar systems," *R&D Rev. Toyota CRDL*, vol. 37, no. 2, pp. 7–12, 2002.
[8] M. Barba, "A high-isolation, wideband and dual-linear polarization patch antenna," *IEEE Trans. Antennas Propag.*, vol. 56, no. 5, pp. 1472–1476, May 2008.
[9] B. Lee, S. Kwon, and J. Choi, "Polarisation diversity microstrip base station antenna at 2 GHz using t-shaped aperture-coupled feeds," *IEE Proc. Microw. Antennas Propag.* , vol. 148, no. 5, pp. 334–338, Oct. 2001.
[10] B. Li, Y.-Z. Yin, W. Hu, Y. Ding, and Y. Zhao, "Wideband dual-polarized patch antenna with low cross polarization and high isolation," *IEEE Antennas Wireless Propag. Lett.*, vol. 11, pp. 427–430, Apr. 2012.
[11] R. Bayderkhani and H. Reza Hassani, "Wideband and low sidelobe slot antenna fed by series-fed printed array," *IEEE Trans. Antennas Propag.*, vol. 58, no. 12, pp. 3898–3904, Dec. 2010.
[12] T. Metzler, "Microstrip series arrays," *IEEE Trans. Antennas Propag.*, vol. AP-29, no. 1, pp. 174–178, Jan. 1981.
[13] T. Yuan, N. Yuan, and L.-W. Li, "A novel series-fed taper antenna array design," *IEEE Antennas Wireless Propag. Lett.*, vol. 7, pp. 362–365, Oct. 2008.
[14] D. M. Pozar and D. H. Schaubert, "Comparison of three series fed microstrip array geometries," in *Proc. IEEE Antennas Propag. Soc. Int. Symp. Dig.*, Ann Arbor, MI, USA, Jun. 1993, vol. 2, pp. 728–731.
[15] J. Huang, "A parallel-series-fed microstrip array with high efficiency and low cross-polarization," *Microw. Opt. Technol. Lett.*, vol. 5, no. 5, pp. 230–233, May 1992.
[16] CST studio suite, 2012 [Online]. Available: http://www.cst.com
[17] D. M. Pozar, *Microwave Engineering*, 3rd ed. New York, NY, USA: Wiley, 2004.
[18] K. Gupta, R. Garg, and R. Chadha, *Computer Aided Design of Microwave Circuits*. Norwood, MA, USA: Artech House, 1981.
[19] Y.-B. Jung, J. H. Choi, and C. W. Jung, "Low-cost K-band patch array antenna for high-sensitivity EM sensor," *IEEE Antennas Wireless Propag. Lett.*, vol. 9, pp. 982–985, 2010.

Fang-Yao Kuo (S'08) was born in Taichung, Taiwan, in 1986. He received the B.S. and M.S. degrees in communications engineering from Yuan Ze University, Chungli, Taiwan, in 2008 and 2010, respectively. He is currently working toward the Ph.D. degree in communications engineering at National Chiao-Tung University, Hsinchu, Taiwan.

His research interests include antenna design and periodic structure for absorbers.

Ruey-Bing (Raybeam) Hwang (M'96–SM'06) received the B.S. degree from the Department of Communications Engineering, National Chiao-Tung University, Hsinchu, Taiwan, in 1990, the M.S. degree from the Department of Electrical Engineering, National Taiwan University, Taipei, Taiwan, in 1992, and the Ph.D. degree from the Institute of Electronic Engineering, National Chiao-Tung University in 1996.

From August 2004 to July 2005, he was an Assistant Professor at the Communication Engineering Department, National Chiao-Tung University. He became a Professor of electrical engineering in August 2008. In August 2013, he was appointed Director of the Institute of Communications Engineering, which is affiliated with the Electrical and Computer Engineering Department. He has authored or coauthored over 100 journal and international conference publications in the area of microwaves, optics, and applied physics. Additionally, he authored a book entitled *Periodic Structures: Mode-Matching Approach and Applications in Electromagnetic Engineering* (Wiley-IEEE Press, 2013). His research interests include phased-array technology (beam-forming and angle-of-arrival estimation), frequency-modulated continuous-wave (FMCW) radar systems, and electromagnetic periodic structure theory.

Prof. Hwang is currently the Chair of IEEE AP-S Taipei Chapter. He is a honorary member of Phi Tau Phi.